ACS APPLIED NANO MATERIALS

www.acsanm.org
Article

Protein-only Nanoparticles for T Cell Expansion and Activation

Marc Fornt-Suñé, Gonzalo Lázaro Bermejo, Marcos Gil-Garcia, Andrea Aran, Javier Garcia-Pardo,* Mercè Martí,* and Salvador Ventura*

Cite This: ACS Appl. Nano Mater. 2024, 7, 6669−6680
Read Online

ABSTRACT: The in vitro expansion and activation of T cells utilizing synthetic nanosized artificial antigen presenting cells (aAPCs) have emerged as a promising technique for cancer treatment. Although diverse nanomaterials have been explored as aAPC scaffolds, protein-only nanoparticles have been largely overlooked, despite their high designability and biocompatibility. In this study, we exploit a plug-and-play approach for the development of protein-only nanoparticles as aAPCs using the self-assembling properties of ZapB coiled coil and the Z-domain antibody-capturing ability. The resulting coiled coil-based nanoparticles (ccNPs) can be easily, rapidly, and simultaneously functionalized with anti-CD3 and anti-CD28 antibodies (ccNPs-CD3/CD28). Our results demonstrate that ccNPs-CD3/CD28 induce polyclonal T cell proliferation and activation while sustaining cytokine production for an extended period. The biocompatibility, modularity, and chemistry-free surface modification of this protein-only strategy render it a versatile platform for in vitro T cell expansion and activation.

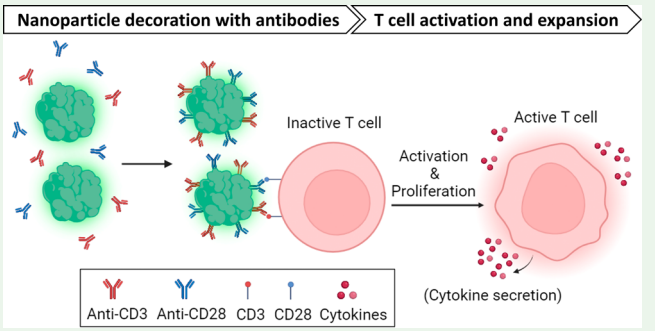

KEYWORDS: *protein nanoparticles, self-assembly, coiled coil, Z-domain, antibody, T cell activation, T cell proliferation*

INTRODUCTION

T cell-based immunotherapy is a promising medical strategy for treating cancer, including metastatic stages or relapsed disease.[1] Adoptive T cell immunotherapy (ACT) involves the transfusion of ex vivo autologous functional T cells.[2] Effective T cell expansion and activation to improve the patient's immune response is crucial to this strategy.[3] T cell activation occurs after recognition by the specific T cell receptor (TCR) of the antigen presented by an antigen-presenting cell (APC). The TCR is associated with CD3, an hexameric complex responsible for the intracellular signaling after antigen recognition.[4] Besides, other interactions are required for the T cell full activation, mainly costimulatory signals produced by the interaction of CD28 on T cells and its ligands, CD80/86, expressed on APCs.[5,6] Thus, polyclonal activation of T cells through TCR can be mimicked in vitro by displaying simultaneously antihuman CD3 and CD28 antibodies acting as receptors' ligands.[7]

One aim of immunotherapy is to tune the immune response in situ. This is achieved by the administration of tumor infiltrating lymphocytes (TILs) expanded in vitro with APCs. Therefore, a challenge in ACT is producing tailored APCs to stimulate antitumor T cells. In this context various synthetic artificial antigen-presenting cells (aAPCs) have been created as an alternative to natural APCs,[8−11] often by grafting T-cell ligands onto the surface of biocompatible materials.[12−14] Different nano- and microstructures including liposomes, exosomes, polymers, gold and magnetic microbeads, mesoporous silica, and DNA origami have been used in these efforts.[15−19] Most of these strategies involve covalently linking activating antibodies (Abs) for CD3 (TCR stimulus) and CD28 (costimulatory cue) to the material through consecutive chemical conjugation steps. However, this process can potentially modify the antibody structure and function. Alternatively, the material surface is biotinylated and avidin conjugated antibodies are employed; providing modularity and the ability to select different costimulatory cues.[20,21] Nevertheless, this approach is expensive and still requires covalent modification of the antibodies.

Here, we make use of protein-only nanoparticles that can be recombinantly produced at preparative levels and easily functionalized with antibodies for different applications, including polyclonal expansion and activation of T cells. Coiled coils are characterized by an arrangement of two or more α-helices into a superhelix, and they are abundant structural motifs in nature, as they are found in many fibrous proteins and transcription factors. Additionally, some coiled coils have self-assembling properties that allow them to interact

Received: February 1, 2024
Revised: February 16, 2024
Accepted: February 19, 2024
Published: February 29, 2024

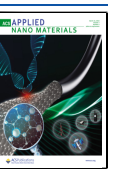

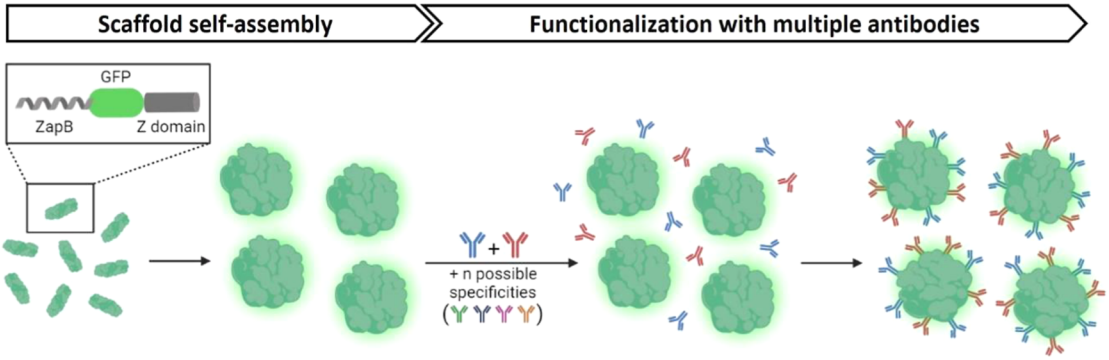

Figure 1. Depiction of the self-assembly and dual-antibody functionalization process of ccNPs. The ZapB-GFP-Z fusion protein is overexpressed in *Escherichia coli* (*E. coli*) and intracellularly self-assembles into coiled coil-based fluorescent protein nanoparticles with antibody-capturing properties. After purification, the resultant nanostructured scaffolds can be readily loaded with a precise combination of antibodies for bispecific and potentially multispecific ligand targeting. In the present work, the ccNPs were functionalized with anti-CD3 and anti-CD28 antibodies, colored in red and blue, respectively, to be used for T cell expansion and activation.

with each other and form higher-order protein structures.[22] Hence, this fold is of significant interest for rational protein design, as it can be used as a building block to create novel protein-based nanostructures. We exploited the self-assembling properties of ZapB, a natural antiparallel coiled coil-forming prokaryotic protein,[23] to build α-helical sustained nanostructures that can be readily purified from microbial cell factories in a preassembled state. This strategy relies on the creation and expression of a tripartite fusion protein, named ZapB-GFP-Z, which consists of ZapB as the coiled coil scaffolding unit, the green fluorescent protein (GFP) as a tracer, and the Z-domain as an antibody-capturing moiety. The Z-domain is a small (6.5 kDa) engineered analogue of the B-domain of protein A that folds into a three-helix bundle[24] and binds immunoglobulins G (IgGs) noncovalently, with nanomolar affinity.[25] As a result, when the ZapB-GFP-Z fusion protein is recombinantly expressed, ZapB drives its spontaneous assembly into spherical scaffolds that behave as fluorescent antibody-capturing nanoparticles. We have shown previously that these protein-only particles can be used to recognize specific cellular types.[26]

Here, in a proof-of-concept study, we tested the ability of our coiled coil-based protein nanoparticles (ccNPs) to act as aAPCs in vitro by decorating them with anti-CD3 and anti-CD28 antibodies. The self-assembly and dual-antibody functionalization process of the ccNPs are illustrated in Figure 1. These bispecific protein-only particles were capable of effectively expanding and activating T cells from human peripheral blood mononuclear cells (PBMCs). The biocompatibility, modularity, and chemistry-free surface modification of our system, combined with the easy production and purification of ready-to-use ccNPs, offer an alternative, scalable, and cost-effective platform for polyclonal expansion of T cells.

MATERIALS AND METHODS

Plasmids and Cells. The codon-optimized synthetic gene of ZapB-GFP-Z was produced by Genscript (USA). The ZapB-GFP-Z sequence was inserted into a pET-28a(+) vector using NcoI and *Bam*HI cloning sites. For the preparation of the IgG-ccNP complexes, both murine antibodies against human CD3 (clone OKT3) and CD28 (clone CD28.2) were purchased from Invitrogen (USA). PBMCs of healthy donors were purified from blood obtained at the Autonomous University of Barcelona Health Care Service with previous consent. PBMC were obtained by centrifugation of 1:1 diluted blood with PBS using Ficoll−Paque density gradient (Lymphoprep; Alere Technologies) at 600*g* for 30 min without brake at room temperature (RT). PBMCs from the interphase between plasma and the Ficoll−Paque were collected and washed twice with PBS by centrifugation at 300*g* for 5 min at RT. Purified PBMCs were cryopreserved in fetal calf serum with 10% of DMSO media and stored in liquid nitrogen until use.

Protein Expression and Purification. For the production of ZapB-GFP-Z coiled coil-based protein nanoparticles (ccNPs), *E. coli* BL21 (DE3) competent cells (Invitrogen, Waltham, USA) were transformed with the previously mentioned plasmid and grown aerobically in 20 mL of Luria−Bertani broth (LB) medium supplemented with 50 μg/mL kanamycin. Cells were incubated on shakers at 37 °C and 250 rpm until the cell density reached an absorbance at 600 nm (OD600) of 0.6. Then, protein expression was induced with 1 mM isopropyl-D-1- thiogalactopyranoside (IPTG) for 6 h at 30 °C and under agitation at 250 rpm. Afterward, cells were collected by centrifugation at 2500 rcf for 20 min and stored at −80 °C until ccNP purification. The cell pellets were resuspended in 1 mL of buffer A (50 mM Tris and 100 mM NaCl, pH 7.4) supplemented with 1 mM PMSF and 150 μg/mL lysozyme. The cells were incubated for 1 h at 37 °C and then were sonicated for 3 min at 15% amplitude in 1 s ON − 1 s OFF cycles, while kept cold on ice. Next, 10 μL of Nonidet P40 Substitute was added to the sonicated cells followed by an incubation of 1 h at 4 °C. Then, 30 μL of 1 M MgSO4 and 25 μL of 1 mg/mL DNase I were added, and the mixture was incubated for 45 min at 37 °C. All incubations were performed under constant agitation. Afterward, the mixture was centrifuged at 15,000 rcf for 15 min at 4 °C. The ccNPs-containing pellet was washed three times with 500 μL of buffer A containing 0.5% Triton X-100 and one time with 500 μL of buffer A containing 2% Triton X-100. Finally, one additional washing step was performed with buffer A alone to remove the remaining detergent from the purified ccNPs. The purity of the ccNPs was checked by SDS-PAGE, and protein concentration was assessed by measuring the absorbance at 280 nm of an aliquot of pure ccNPs dissolved in 6 M guanidine hydrochloride using a Specord 200 Plus spectrophotometer (Analytik Jena, Jena, Germany).

Preparation of Antibody-Decorated ccNPs. The IgG-ccNP complexes were obtained by incubating 50 μL of 25 μM ccNPs with 1 μg of the indicated IgGs for 45 min at RT. To obtain the anti-CD3 monospecific ccNPs, 1 μg of anti-CD3 antibody was incubated with the particles. The anti-CD3 + anti-CD28 bispecific ccNPs were prepared by mixing 0.5 μg of each antibody with the particles. To achieve efficient antibody conjugation, the samples were mixed every 5 min. After incubation, the antibody-loaded ccNPs were centrifuged at 15000 rcf for 20 min and resuspended in 100 μL of buffer A (50 mM Tris and 100 mM NaCl, pH 7.4) to remove the excess of unbound antibodies. Then, the sample was centrifuged again under the same conditions and resuspended in 50 μL of buffer A to obtain the IgG-ccNP complexes that were further used in T cell proliferation

https://doi.org/10.1021/acsanm.4c00698
ACS Appl. Nano Mater. 2024, 7, 6669−6680

assays. Unloaded control ccNPs or naive ccNPs were prepared as control conditions following the same procedure but without incubation with antibodies.

Scanning Electron Microscopy. The structural properties of the ccNPs were investigated by scanning electron microscopy (SEM). 5 μL aliquots at a concentration of 5 μM of the ccNPs were prepared in buffer A (50 mM Tris and 100 mM NaCl, pH 7.4). The samples were directly placed on silicon wafers (Ted Pella Inc., Redding, USA), dried under N_2 flow, and observed using a Field Emission Merlin scanning electron microscope (Zeiss Merlin, Oberkochen, Germany) operating at a voltage of 1 kV and employing the secondary electron detector. Image analysis and size measurements were performed with ImageJ software.[27]

Dynamic Light Scattering. Samples of both naive ccNPs and antibody decorated ccNPs were prepared to a final concentration of 25 μM ccNPs in buffer A (50 mM Tris and 100 mM NaCl, pH 7.4). The antibody decorated ccNPs were prepared as detailed in the "Preparation of Antibody-Decorated ccNPs" section. Mean particle size of the ccNPs samples was determined by dynamic light scattering (DLS) using a Zetasizer Nano S90 (Malvern Panalytical, Malvern, UK) at 25 °C. All the measurements were performed in the automatic mode, as an average of 12 runs.

To monitor the stability of ccNPs over time, samples of both naive ccNPs and antibody decorated ccNPs were prepared to a final concentration of 2.5 μM in buffer A (50 mM Tris and 100 mM NaCl, pH 7.4) containing sodium azide 0.01%. The antibody-decorated ccNPs were prepared as detailed in the "Preparation of Antibody-Decorated ccNPs" section. The samples were incubated at RT under mild agitation for 5 days, and mean particle size of ccNPs was determined by DLS every 24 h using a Zetasizer Nano S90 (Malvern Panalytical, Malvern, UK).

Fourier-Transform Infrared Spectroscopy. For secondary structure analysis, the ccNPs were analyzed by FTIR using a Bruker Tensor 27 FTIR (Bruker Optics, Billerica, USA) supplied with a Specac Golden Gate MKII ATR accessory. To perform measurements, the ccNPs were resuspended in buffer A (50 mM Tris and 100 mM NaCl, pH 7.4), deposited on the ATR crystal, dried under N_2 flow, and 32 scans were acquired at a resolution of 1 cm^{-1} within the 1800−1500 cm^{-1} range. The recorded spectral data were processed and normalized using the OPUS MIR Tensor 27 software (Bruker Optics, Billerica, USA) and subsequently fitted using PeakFit Software (Systat Software) to obtain the final ccNPs FTIR spectrum.

Fluorescence Spectroscopy. Samples of 50 μL of 5 μM ccNPs were prepared in buffer A (50 mM Tris and 100 mM NaCl, pH 7.4), and the fluorescence excitation and emission spectra of GFP were measured in a Jasco FP-8200 fluorescence spectrofluorometer (Jasco Corporation, Japan). All fluorescence spectra were recorded using the following spectrofluorometer settings: Excitation and emission bandwidths: 5 nm. Response: 0.5 s. Sensitivity: high. Data interval: 0.5 nm. Scan speed: 1000 nm/min. Accumulations: 3. Measurement range: 420−520 nm for excitation spectra (excitation mode and emission wavelength: 535 nm) and 480−580 nm for emission spectra (emission mode and excitation wavelength: 460 nm).

For antibody loading capacity determination, 50 μL of 5 μM ccNPs were incubated with 1 μg of two fluorescent secondary antibodies, one labeled with AF555 (AF555-IgG) and the other one labeled with AF647 (AF647-IgG) at a 1:1 ratio, and the sample was processed as detailed in the "Preparation of Antibody-Decorated ccNPs" section. Next, the fluorescence emission spectra of AF555 and AF647 were measured in the samples containing the antibody-decorated ccNPs using a Jasco FP-8200 fluorescence spectrofluorometer (Jasco Corporation, Japan). Then, calibration curves were elaborated for AF647-IgG and AF555-IgG. A series of dilutions of each antibody were prepared at growing concentrations (0/0.1/0.25/0.5/1/2.5/5 ng/μL) and their fluorescent signal was measured. The fluorescence emission maxima were plotted as a function of protein concentration to obtain the corresponding calibration curve for each labeled antibody. Finally, the fluorescent signals obtained for the antibody decorated ccNPs were interpolated to their respective calibration curve and the amount of labeled antibody captured on the surface of ccNPs was calculated. All fluorescence spectra were recorded using the following spectrofluorometer settings: excitation and emission bandwidths: 5 and 10 nm, respectively. Response: 0.5 s. Sensitivity: high. Data interval: 1 nm. Scan speed: 500 nm/min. Accumulations: 3. Measurement range: 553−600 nm for AF555 (emission mode and excitation wavelength: 540 nm) and 645−720 nm for AF647 (emission mode and excitation wavelength: 630 nm).

Flow Cytometry. For the preparation of antibody-decorated ccNPs, 50 μL of 5 μM ccNPs were incubated with 1 μg of two fluorescent secondary antibodies, a CF350-labeled IgG and a CF555-labeled IgG, for 45 min at RT. To obtain ccNPs decorated with a single fluorescent antibody, 50 μL of 5 μM ccNPs were incubated with 1 μg of either CF350-IgG or CF555-IgG. To obtain the double antibody decorated ccNPs, 50 μL of 5 μM ccNPs was incubated with both antibodies simultaneously at a 1:1 ratio (0.5 μg of CF350-IgG + 0.5 μg of CF555-IgG). The samples were mixed every 10 min. After incubation, the antibody-loaded ccNPs were centrifuged at 15000 rcf for 20 min to remove the excess of unbound antibodies, and the pellets were resuspended again in buffer A (50 mM Tris and 100 mM NaCl, pH 7.4) to a final ccNP concentration of 0.375 μM. Also, naive ccNPs were prepared as a control following the same procedure but without incubation with antibodies. Finally, the samples were analyzed in a CytoFLEX LX flow cytometer (Beckman Coulter Life Sciences, USA) to detect colocalization of the CF350/CF555 fluorescence of the labeled antibodies with the GFP fluorescence of ccNPs.

For antibody release determination, samples of ccNPs decorated with CF350-IgG and CF555-IgG were prepared as previously described and were subsequently incubated at RT for 24 h. Afterward, the samples were centrifuged at 15,000 rcf for 20 min to remove the released antibodies. The resulting pellets containing ccNPs were resuspended again in buffer A to a final concentration of 0.375 μM and were analyzed by flow cytometry as previously indicated. The percentage of naive ccNPs present in the samples was determined and compared with that of freshly prepared samples.

Confocal Microscopy. For confocal microscopy analysis, 50 μL of 5 μM ccNPs were incubated with 1 μg of two fluorescent secondary antibodies, one labeled with Alexa Fluor 555 (Ab-AF555) and the other one labeled with eFluor 450 (Ab-EF450) at a 1:1 ratio, and the sample was processed as detailed in the "Preparation of antibody-decorated ccNPs" section. The resulting double antibody decorated ccNPs were placed on top of a microscopy glass slide and covered with a coverslip. Confocal fluorescence images were obtained with a Leica SP5 confocal microscope (Leica Microsystems, Germany). The fluorescence intensity of the different fluorophores was observed exciting the sample at 410 and 555 nm for eFluor 450 and Alexa Fluor 555, respectively.

Colloidal Gold Immunolabeling and Transmission Electron Microscopy. A suspension containing 5 μM ccNPs was mixed with an antimouse 10 nm colloidal gold-linked secondary antibody (1:50 dilution) in buffer A (50 mM Tris, 100 mM NaCl, pH 7.4) and was incubated for 1 h at RT. Afterward, the sample was centrifuged at 15000 rcf for 20 min and resuspended again in buffer A to remove the excess of unbound antibodies. Then, 5 μL of the sample were deposited on EMR 400 mesh carbon-coated copper grids (Micro to Nano Innovative Microscopy Supplies) and incubated for 5 min. Excess solutions were removed with a filter paper. Next, the grids were washed with 10 μL of MQ water, allowed to dry, and observed using a JEOL JEM1400 Electron Microscope operating at 120 kV and equipped with a CCD GATAN 794 MSC 600HP camera. Representative micrographs were recorded at two different magnifications (i.e., ×3000 and ×5000) and images were processed using ImageJ.[27]

LPS Quantification. ccNPs were dispersed in pyrogen-free H_2O to a final concentration of 25 μM. Then, the levels of LPS present in the ccNPs samples were quantified using the Pierce Chromogenic Endotoxin Quant Kit (ThermoFischer scientific, Massachusetts, USA) following the instructions provided by the manufacturer.

T Cell Proliferation Assay. PBMCs from four healthy donors were used as responder cells to monitor the proliferation. PBMCs

https://doi.org/10.1021/acsanm.4c00698
ACS Appl. Nano Mater. 2024, 7, 6669−6680

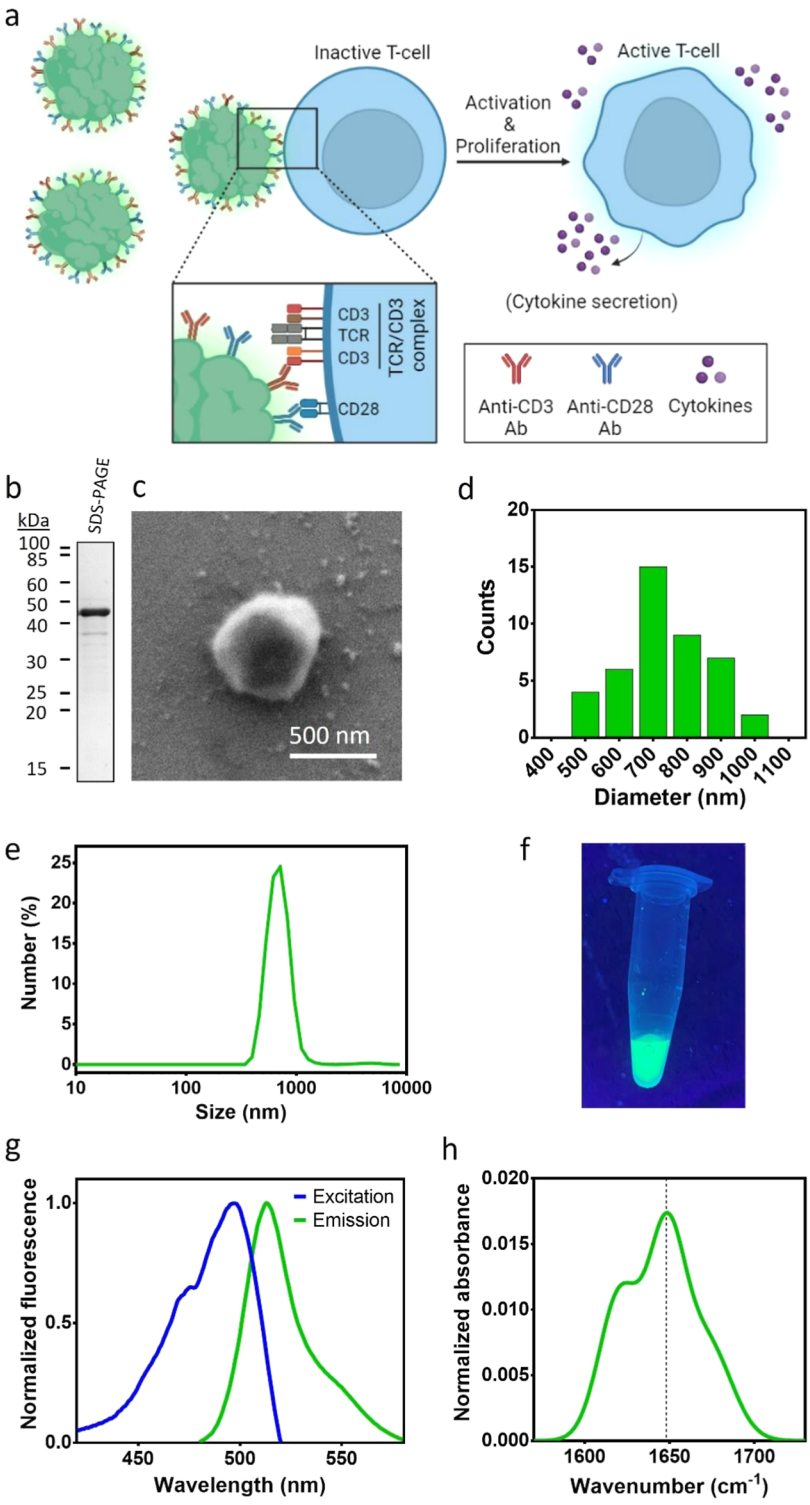

Figure 2. Biophysical characterization of ccNPs. (a) Graphical representation of human T cell activation and expansion promoted by ccNPs decorated with anti-CD3 and anti-CD28 antibodies. The zoomed-in inset depicts the nanoparticle-T cell interface, in which the stimulating antibodies displayed by ccNPs interact with their respective receptors in human T cells. (b) SDS-PAGE of purified ccNPs. (c) SEM micrograph of a ccNP. (d) Size distribution of different ccNPs spotted in SEM micrographs. (e) Size distribution of ccNPs measured by DLS. (f) ccNPs dispersed in a physiological buffer and displayed green fluorescence under an ultraviolet light source. (g) Fluorescence excitation (blue) and emission (green) spectra of ccNPs measured by fluorescence spectroscopy. (h) Secondary structure analysis of ccNPs by FTIR spectroscopy. The dotted line indicates the α-helix band at 1648 cm^{-1}.

were labeled with 5 μM cell proliferation dye eFluor 670 (Invitrogen, Life Technologies, Thermo Fisher Scientific, USA) according to the manufacturer protocol. Labeled responder cells were seeded at 30,000 cells/well in 96-well round-bottom plates in a final volume of 200 μL of complete medium [IMDM GlutaMAX (Gibco) complemented with 10% of decomplemented human serum, 1X antibiotic-antimycotic (Gibco) and IL-2 at 40 U/ml] in the presence of 50,000 irradiated (30 Gy) PBMCs as feeder cells. Naive ccNPs,

https://doi.org/10.1021/acsanm.4c00698
ACS Appl. Nano Mater. 2024, 7, 6669−6680

ccNPs-CD3, and ccNPs-CD3/CD28 were added at a final concentration of 2,5 μM. Before selecting this concentration, a preliminary assay was conducted to test T cell proliferation using ccNPs-CD3/CD28 at different concentrations (2.5 μM, 5 μM, and 10 μM). The ccNPs concentration of 2.5 μM was selected as the condition that provided a close to maximum response, while minimizing the amount of ccNPs.

As controls, PBMCs were cultured in the presence of antihuman CD3/anti-CD28-coated Dynabeads (Gibco) at a ratio of 1bead:10 labeled PBMCs (positive control) and without any stimulus (negative control). The Dynabead-to-cell ratio of 1:10 was selected as it proved to achieve T cell proliferation levels higher than 90%, as well as make the retrieval of the beads unnecessary.

Each condition was seeded in triplicate, and after 5 days of culture, cells were harvested, and proliferation was analyzed in a CytoFLEX S flow cytometer (Beckman Coulter Life Sciences, USA). Percentage of divided cells was calculated using FlowJo 10.4 software (TreeStar, Ashland, USA).

Phenotype and Activation of PBMCs. PBMCs from two healthy donors were used to monitor the expansion of PBMCs populations and T cell activation in the presence of the different stimuli used in the proliferation assays. At day 0 and after 5 days of culture, cells were stained with antihuman antibodies for 20 min at 4 °C in the dark with PBS containing 2% FBS. After incubation, cells were washed twice, collected in 200 μL of PBS, and analyzed by flow cytometry. The antibodies used for the characterization of the expanded populations were PerCP-conjugated anti-CD3 (BD Biosciences), PE-conjugated anti-CD19 (BD Biosciences), and FITC-conjugated anti-CD14 (Miltenyi Biotec). To assess T cell activation, PE-Cy5-conjugated antiCD25 (BD Biosciences) and FITC-conjugated anti-HLA-DR (BD Biosciences) were used. Cell acquisition and analysis were performed with the flow cytometer CytoFLEX S (Beckman Coulter Life Sciences, USA), and the FlowJo 10.4 software (TreeStar, Ashland, USA), respectively.

Cytokine Detection. Supernatants from the proliferation assays (n = 4) were collected on day 5 of culture and stored at −20 °C until the measurement of cytokine production. The secretion of TNF-α, IL-10, IFN-γ, IL-4, IL-17A, sFas, sFasL, granulysin, perforin, granzyme A, and granzyme B was analyzed by using the LEGENDplex Human CD8/NK Panel (Biolegend), according to the manufacturer's instructions. Briefly, a mix of beads differentiated by size and internal fluorescence intensities and conjugated with a specific antibody were incubated with the supernatants. After the plates were washed, a biotinylated detection antibody cocktail—specific for the same cytokines—was added. Finally, streptavidin-phycoerythrin was subsequently added, providing fluorescent signal intensities in proportion to the analytes bound to the beads. The addition of a standard solution for each cytokine was included, which led us to quantify the analyte. The multiplexed assay was analyzed in a CytoFLEX S flow cytometer (Beckman Coulter Life Sciences, USA) and quantitative analysis was performed using standard curve-plotting software (LEGENDplex Data Analysis Software Suite) to determine the concentration for each analyte.

Statistical Analysis. Statistical analysis for the different assays was performed using GraphPad Prism 7.0 software (GraphPad Software Inc.). The differences between all conditions were compared using ordinary one-way ANOVA according to Turkey multiple comparison post hoc test. Note that the statistical significance of each experiment is reported in the figure legend.

RESULTS AND DISCUSSION

Preparation and Characterization of Antibody Decorated ccNPs. The current study exploits ccNPs as a platform for the simultaneous delivery of anti-CD3 and anti-CD28 antibodies (Abs) to promote in vitro T cell activation (Figure 2a). The ZapB-GFP-Z fusion protein was recombinantly expressed in *E. coli*. The ZapB moiety mediates the spontaneous and rapid self-assembly of the fusion protein in the cytosol into ccNPs. As ZapB is sequentially connected to GFP and the Z-domain, these functional modules are also accommodated in the resulting nanostructures. GFP allows particle tracking through fluorescence, whereas the Z-domain endorses the system with a high affinity and specificity for immunoglobulins. ccNPs were purified from the insoluble cell fraction as previously described,[26] and a washing step with 2% Triton X-100 was included to eliminate residual lipopolysaccharides (LPS). The yield was ∼150 mg protein/L culture, with no major protein contaminants observed in the purified particles when analyzed by SDS-PAGE (Figure 2b). SEM images revealed that purified ccNPs were spherical submicrometer particles with an average diameter of 787.6 ± 131.5 nm (Figure 2c,d). This size is in good agreement with DLS measurements of the same sample dispersed in a physiological buffer, which showed a hydrodynamic diameter of 697.1 ± 162.7 nm (Figure 2e).

ccNPs are reminiscent of bacterial inclusion bodies (IBs) but differ in their assembly mechanism. Unlike conventional IBs, ccNPs are not sustained by the formation of intermolecular β-sheets of an amyloid-like nature between misfolded and thus mostly inactive polypeptide chains,[28] but instead by the assembly of native α-helical structures, which are not expected to significantly impact the fold of the adjacent proteins.[29] Consistent with this view, purified ccNPs are highly fluorescent and display fluorescence excitation and emission spectra equivalent to those of native GFP (Figure 2f,g). Additionally, the Fourier transform infrared (FTIR) spectroscopy spectrum in the in the amide I region (1600−1700 cm^{-1}) show a dominant signal at 1648 cm^{-1}, which can be attributed to the α-helical structures of the ZapB and Z domains, and which is absent or minor in conventional IBs[30] (Figure 2h).

The functionality of the Z-domain in ccNPs was assessed by monitoring their simultaneous binding to two distinct antibodies labeled with different fluorophores by confocal fluorescence microscopy. Alexa Fluor 555 (AF555) and eFluor 450 (EF450), were used as labels, producing red and blue fluorescence emissions, respectively. As depicted in Figure S1a, the green fluorescence from GFP, as well as red and blue fluorescence from the two labeled antibodies, colocalized in ccNPs. It is noteworthy that such antibody functionalization was achieved in situ through noncovalent interactions, following a simple procedure that can be completed within 1 hour without the use of any chemical reagents (see Materials and Methods section). The antibody loading capacity of ccNPs was assessed by decorating the protein nanoparticles with fluorescent antibodies, labeled with either AF555 (AF555-Ab) or AF647 (AF647-Ab) and measuring the retained fluorescence by spectrofluorometry. The ccNPs exhibited an antibody loading capacity of 4.85 ± 1.31 ng of AF555-Ab per μg of ccNPs and of 7.11 ± 1.23 ng of AF647-Ab per μg of ccNPs (Table S1), not being statistically different ($p > 0.5$).

The same approach was used to demonstrate that ccNPs can be simultaneously decorated with different antibodies in the desired ratio simply by incubating them with the chosen antibodies in the selected proportion. To this end, ccNPs were incubated with AF555-Ab and AF647-Ab at a 1:1 ratio, and the fluorescence displayed by the bound antibodies was quantified. The loading of antibodies on ccNPs was 2.72 ± 0.81 ng of AF555-Ab per μg of ccNPs, and 2.73 ± 0.26 ng of AF647-Ab per μg of ccNPs (Table S2). Both antibodies were thus captured in equivalent amounts since the observed loading values were not statistically significant ($p > 0.5$).

https://doi.org/10.1021/acsanm.4c00698
ACS Appl. Nano Mater. 2024, 7, 6669−6680

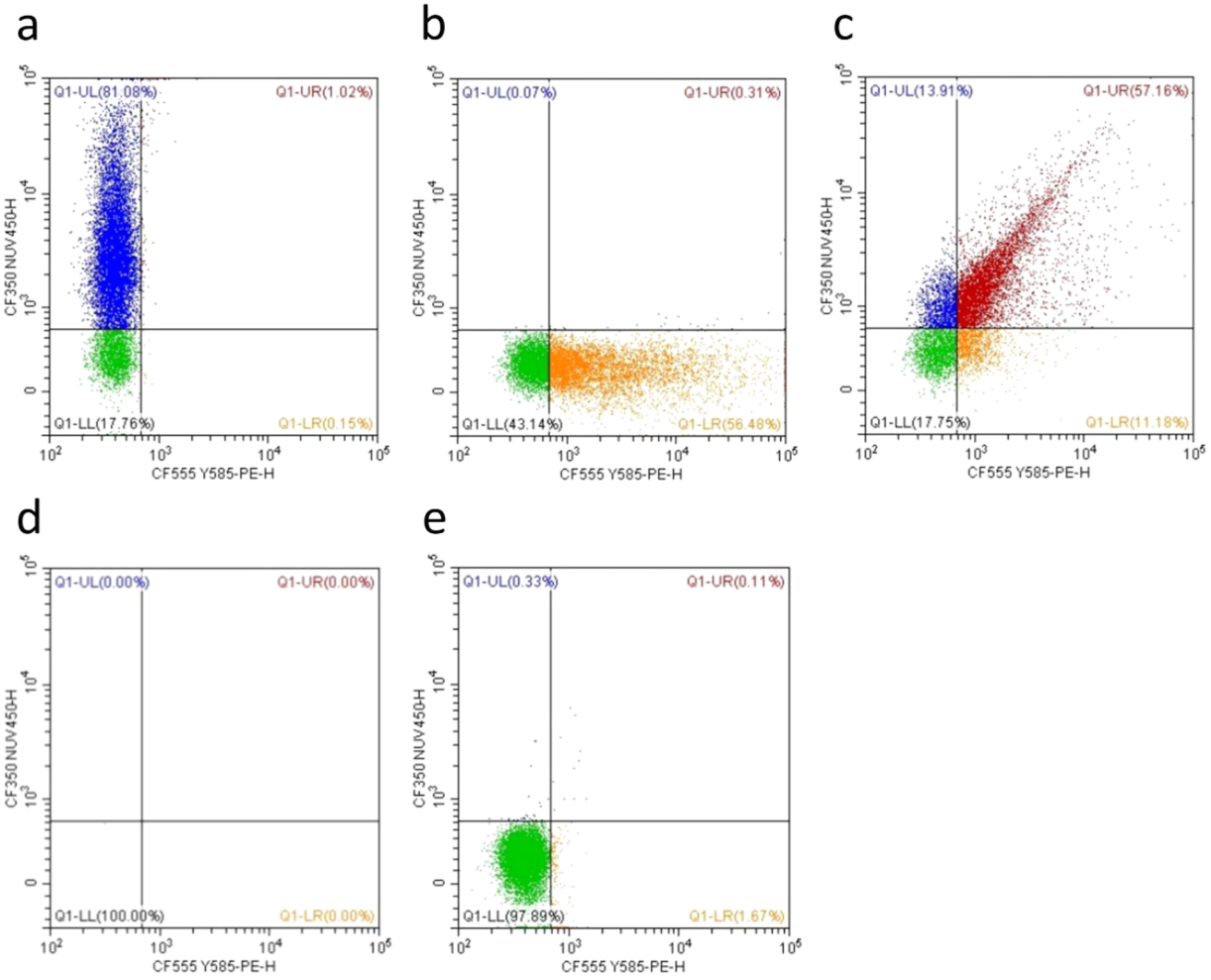

Figure 3. Double antibody functionalization of ccNPs. Flow cytometry scatter plots of (a) ccNPs decorated with a CF350-labeled antibody, (b) ccNPs decorated with a CF555-labeled antibody, (c) ccNPs decorated with both CF350-labeled and CF555-labeled antibodies, (d) the buffer in which the ccNPs are dispersed, and (e) nondecorated or naive ccNPs.

Additionally, we used flow cytometry (FC) to confirm the single and double decoration of ccNPs with fluorescent antibodies (Figure 3). Naive ccNPs emit fluorescence in the green channel, confirming the presence of active GFP, whether the majority of ccNPs decorated with CF350-labeled IgG (CF350-Ab) or CF555-labeled IgG (CF555-ab) emit fluorescence in the blue and orange-red channels, respectively (Figure 3a,b). The majority of ccNPs incubated simultaneously with CF350-Ab and CF555-Ab (>57%) emitted fluorescence in the two channels, ensuring the incorporation of both antibodies into the ccNPs (Figure 3c). Most particles map in the diagonal of the scatter plot, indicating that they are labeled with equivalent amounts of the two fluorescently labeled antibodies. DLS measurements of these double antibody-decorated ccNPs displayed an average hydrodynamic diameter of 705.9 ± 160.4 nm ±0.46 mV, indicating that particle size and homogeneity were not significantly altered by immunoglobulin binding (Figure S2a,b).

ccNPs are not intended for the delivery of free antibodies, and once the antibodies are captured by the nanoparticles, they are not expected to be released from them easily because the noncovalent, but high-affinity interaction with the Z-domain. We monitored the release of antibodies from CF350-Ab and CF555-Ab loaded ccNPs using FC. Upon leaving ccNPs in solution for 24 h, still 95.1% of the antibody remained bound to the nanoparticles.

In a different approach, ccNPs were decorated with antibodies conjugated to 10 nm gold nanoparticles and examined by transmission electron microscopy (TEM). As shown in Figure S1b, the gold nanoparticles were visibly present on the surface of the less electron-dense protein particles. Taken together, these results confirm that the Z-domain modules are also properly folded and functional, rendering multivalent antibody-binding protein nanoparticles.

Zeta potential (ZP) measurements of ccNPs were performed before and after their simultaneous decoration with two different antibodies (anti-CD3 and anti-CD28) (Figure S2c). Naive ccNPs and antibody-bound ccNPs displayed similar ZP values of −9.34 ± 0.19 and −10.23 ± 0.46 mV, respectively. The ZP values are in the range of those of carboxylated polystyrene particles decorated with protein coronas of fibrinogen (−12), albumin (−10) or γ-globulin (−9).[31] While these values suggested that the particles might not be theoretically optimal for their delivery into an organism, they were designed for their in vitro use. Therefore, we explored whether under the conditions and time range in which they will be used for T cell activation, naive ccNPs, and double decorated ccNPs (anti-CD3 + anti-CD28) tended to spontaneously agglomerate. The nanoparticles were left in

https://doi.org/10.1021/acsanm.4c00698
ACS Appl. Nano Mater. 2024, 7, 6669−6680

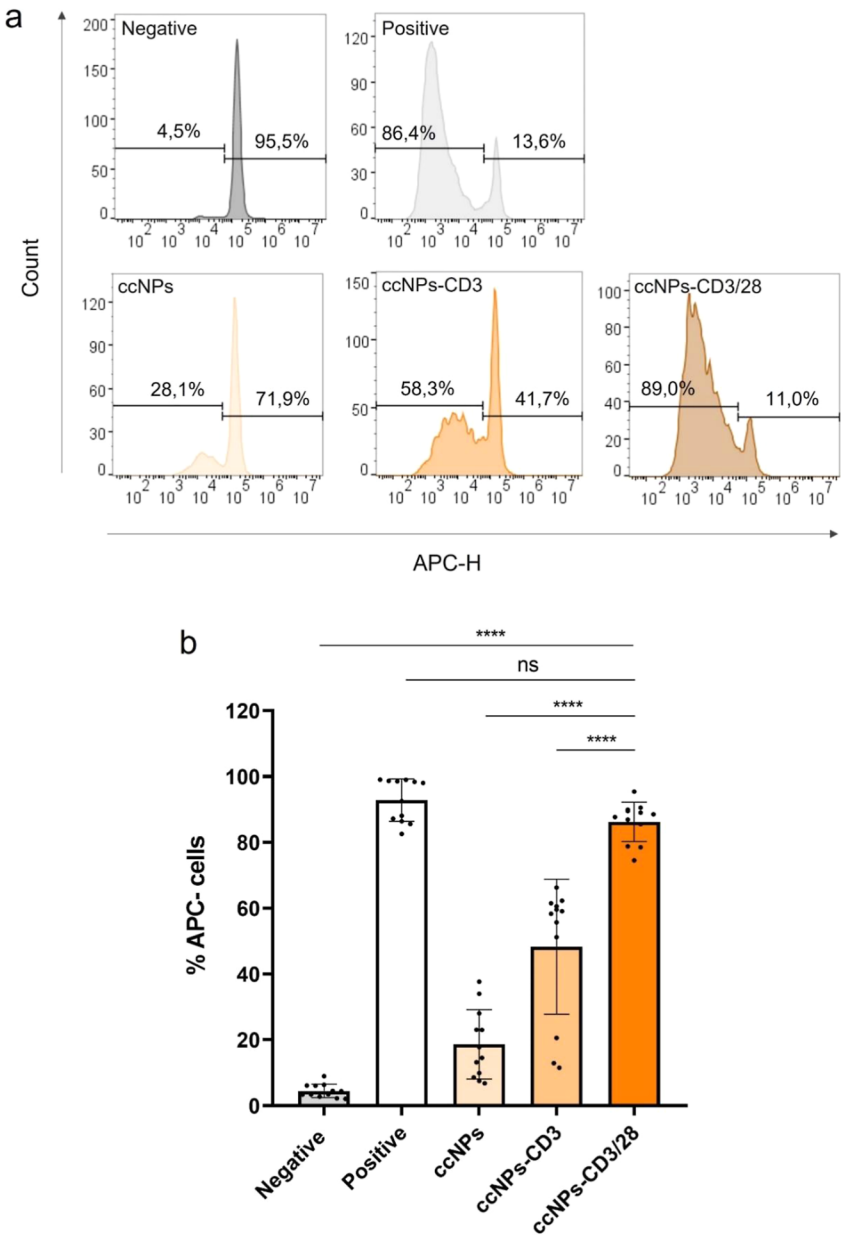

Figure 4. T cell proliferation induced by ccNPs decorated with antihuman CD3 and CD28 antibodies (ccNPs-CD3/CD28). Human PBMCs from different healthy donors were labeled with dye eFluor 670 (5 μM) and cultured for 5 days without stimulus (negative) and in the presence of antihuman CD3/CD28-coated Dynabeads (positive), naive ccNPs, ccNPs-CD3, and ccNPs-CD3/CD28. Percentages of divided cells were measured by the loss of eFluor 670 dye fluorescence (eFluor fluorescence or APC-H) by flow cytometry. Panel a shows representative histograms derived from a single PBMC proliferation assay showing that T cell proliferation was significantly increased in the presence of ccNPs decorated with both antihuman CD3 and CD28 antibodies (ccNPs-CD3/CD28). Panel b shows the average proliferation results with PBMCs from four human healthy donors (n = 4), where % APC- cells shows the percentage of eFluor negative cells and thus indicates proliferation. The assays were performed in triplicate and the error bars show the standard deviation of the mean. One-way ANOVA was performed, followed by Turkey's posthoc multiple comparison test. ****p < 0.0001, compared to the indicated conditions.

solution for 5 days, and the size distribution was monitored daily using DLS. The size of both particles remained unchanged during this time period, indicating that they are colloidally stable in the assay conditions (Figure S3).

Antibody-Decorated ccNPs Properly Stimulate a T Cell Response. Multivalent signaling (i.e., TCR signaling and costimulation) is essential for full T cell activation.[32] We hypothesized that loading the ccNPs with both anti-CD3 and anti-CD28 antibodies might allow them to act as aAPCs in vitro. To test this hypothesis, we performed an e670-proliferation assay using human PBMCs from four healthy donors as responder T cells. PBMCs are heterogeneous cellular mixtures of mononuclear cells primarily composed of monocytes and T cells, from which the majority are naive T cells (CD25- T cells). The assay was designed to evaluate the ability of ccNPs loaded with anti-CD3 and anti-CD28 antibodies in a 1:1 ratio (ccNPs-CD3/CD28) to stimulate T cells. Additionally, we tested ccNPs functionalized with only anti-CD3 antibody (ccNPs-CD3), which only provides TCR signaling, and naive ccNPs to determine their intrinsic T cell activation potential.

https://doi.org/10.1021/acsanm.4c00698
ACS Appl. Nano Mater. 2024, 7, 6669−6680

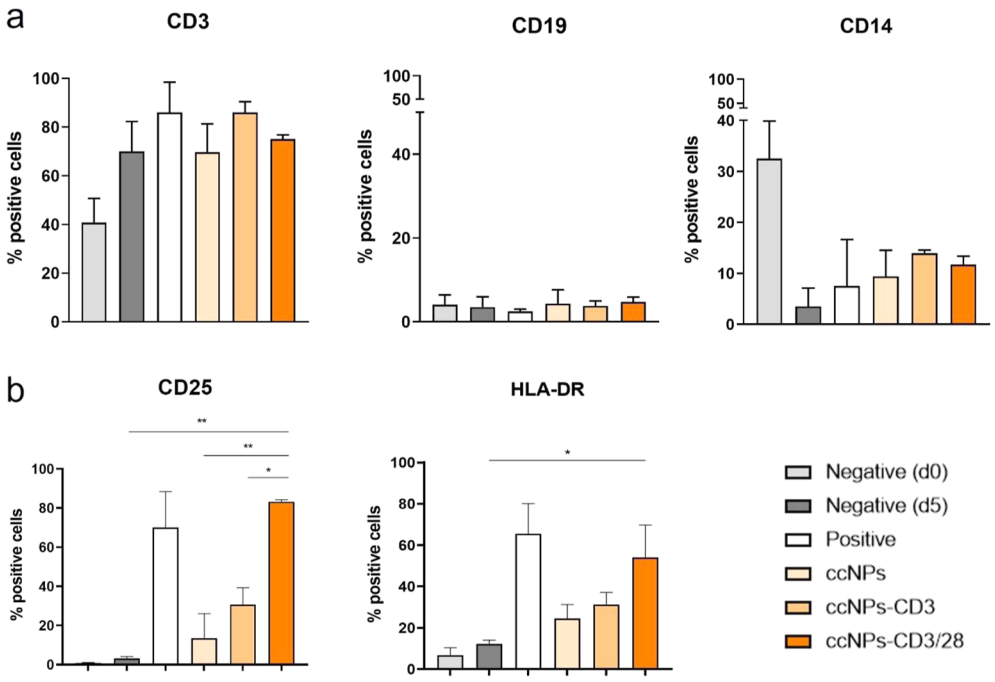

Figure 5. ccNPs decorated with antihuman CD3 and CD28 antibodies induced an efficient T cell activation. Freshly thawed human PBMCs [negative (d0)] and the same PBMCs cultured for 5 days in the different conditions {without stimulus [Negative (d5)] and in the presence of commercial antihuman CD3/CD28 coated Dynabeads (positive), naive ccNPs, ccNPs-CD3, and ccNPs-CD3/CD28} were stained with different antihuman antibodies to evaluate (a) PBMCs phenotype and (b) T cell activation. Here, we represent the percentage of positive cells for the different conditions in all experiments ($n = 2$). The assays were performed in triplicate, and the error bars show the standard deviation of the mean. One-way ANOVA was performed, followed by Turkey's posthoc multiple comparison test. *$p < 0.05$, **$p < 0.01$, compared to the indicated conditions.

The eFluor 670-labeled PBMCs were incubated with medium alone as negative control or with the different ccNP formulations. Antihuman CD3/CD28-coated microbeads (Dynabeads) were used as a positive control. As eFluor 670 binds covalently to proteins, with each cell division the fluorescence intensity is equally distributed among the daughter cells. This allows for a direct correlation between cell proliferation and the loss of eFluor 670 dye signal (from now on eFluor fluorescence intensity, represented as APC-H in Figure 4a). Figure 4a shows an individual proliferation assay, showing the effect of each stimulus on T cell proliferation, measured by the loss of eFluor fluorescence. The average results obtained from proliferation assays with PBMCs from all donors are represented in Figure 4b. The results showed that T cell proliferation induced by ccNPs-CD3/CD28 was comparable to that of the positive control (antihuman CD3/CD28 coated Dynabeads), with more than 80% of the cells undergoing proliferation (Figure 4b). As expected, the presence of both TCR stimulatory (CD3) and costimulatory (CD28) signals were needed for the complete T cell activation, with ccNPs-CD3 inducing a significantly lower level of proliferation than ccNPs-CD3/CD28 ($p < 0.0001$). A significant difference was observed between ccNPs versus ccNPs-CD3 ($p < 0.0001$) and ccNPs versus ccNPs-CD3/CD28 ($p < 0.0001$), indicating that the nanoparticles themselves did not account for the observed differences in T cell expansion. Still, ccNPs alone induced roughly 20% of proliferation, compared with the medium alone (~5%) ($p < 0.05$), which may suggest a certain adjuvant effect of our protein nanoparticles on naive T cell proliferation.

ccNPs-CD3/CD28 Induce the Expression of T Cell Activation Markers. Due to the heterogeneous composition of the PBMCs, it could be that the observed high proliferation in the presence of ccNPs might respond to the expansion of other cell populations, in addition to T cells. PBMCs are mainly represented by T lymphocytes, B lymphocytes, and monocytes. A set of molecular markers defining these cell populations were chosen for a phenotype analysis of the cells expanded in the proliferation assays. CD3 is a component of the TCR complex; therefore, it is present in the surface of T cells. CD19 is a membrane glycoprotein involved in signal transduction of B-cell differentiation and activation. CD14 is a glycosylphosphatidylinositol-linked single-chain surface membrane glycoprotein with a high affinity for lipopolysaccharide (LPS) and is primarily expressed in monocytes.

The phenotype of PBMCs from two healthy donors was analyzed at day 0 (before seeding) and after 5 days of culture in each condition of the proliferation assays. As shown in Figure 5a, ccNPs-CD3/CD28 specifically induced the expansion of T cells since the expression of B-cell (CD19) and monocyte (CD14) markers was considerably low at day 5 of culture. In this way, monocytes, represented by CD14+ cells, accounted for 30% of the initial PBMCs, but this percentage was substantially reduced at day 5 of culture in all conditions. Moreover, transcription of CD14 on human monocytes is highly upregulated by LPS,[33] so we can rule out a significant contribution of residual LPS to T cell activation by ccNPs. To confirm this extent, we quantified endotoxin levels in naive ccNPs using a chromogenic assay that exploits the interaction of endotoxins with proenzyme Factor C. The detected levels were as low as 42.2 pg of LPS/ug of ccNPs.

The low percentage of CD19+ cells (B-cells) at day 0 remained so among all day 5 conditions. Not surprisingly, the

https://doi.org/10.1021/acsanm.4c00698
ACS Appl. Nano Mater. 2024, 7, 6669−6680

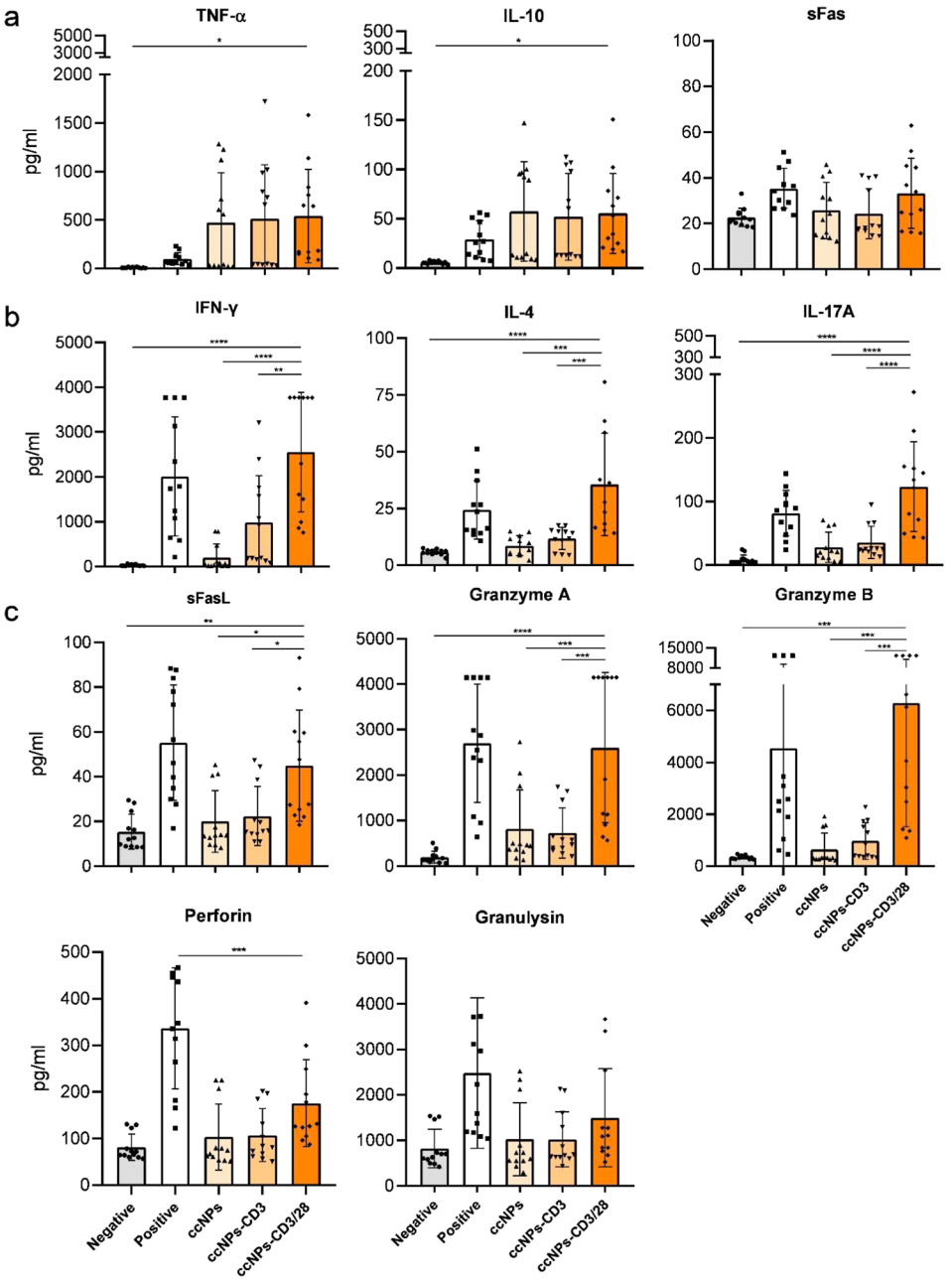

Figure 6. ccNPs decorated with antihuman CD3 and CD28 antibodies induced sustained cytokine and cytotoxic molecules production. PBMCs culture supernatants from proliferation assays (n = 4) (see Figure 4) performed in the presence of different stimuli [without stimulus (negative) and in the presence of commercial antihuman CD3/CD28-coated Dynabeads (positive), naïve ccNPs, ccNPs-CD3, and ccNPs-CD3/CD28] were collected at day 5 of culture. Quantitative analysis was performed using standard curve-plotting software to determine the concentration for each analyte. Values of picograms per milliliter vary between the analytes as the level of production depends on each one. Analytes are grouped according to the producing cell within PBMCs: (a) cytokines produced by PBMCs, (b) cytokines secreted by CD4+ Th cells; IFNγ by Th1 (also produced by CD8+ T cells and residual NK cells), IL-4 by Th2 and IL-17A by Th17, and (c) molecules related with the cytotoxic effector mechanism of CD8+ T cells and residual NK cells, i.e., sFasL, granulysin, perforin, and granzymes A and B. The assays were performed in triplicate and the error bars show the standard deviation of the mean ($p < 0.05$, $^{**}p < 0.01$, $^{***}p < 0.001$, and $^{*}p < 0.0001$).

percentage of CD3+ T cells increased on day 5 of culture in all conditions studied, as the complete culture medium contains human serum and IL-2 that help to maintain the quiescence state and already activated T-cells in the absence of any other stimulus.

To determine whether ccNPs-CD3/CD28 increased efficiently T cell activation levels, we analyzed CD25 and HLA-DR expression patterns (Figure 5b). CD25 corresponds to the α chain of the receptor of IL-2 (IL-2Rα) and is expressed by activated T cells, constituting the high affinity receptor for IL-2 together with the β and γ chains, allowing full activation of T cells. HLA-DR, on the other hand, is an MHC class II molecule induced only in activated T cells. In the analysis, CD3+ T cells were gated to assess the expression of activation markers. Comparison between ccNPs versus ccNPs-CD3/CD28 ($p < 0.01$) and ccNPs-CD3 versus ccNPs-CD3/CD28 ($p < 0.05$) revealed that maximum CD25 expression was achieved upon functionalization with both stimulating cues.

https://doi.org/10.1021/acsanm.4c00698
ACS Appl. Nano Mater. 2024, 7, 6669−6680

The induction of HLA-DR expression displayed the same relationship between types of ccNPs, although the differences were not statistically significant ($p > 0.05$). Overall, percentages of CD25+ and HLA-DR + T cells in the presence of ccNPs-CD3/CD28 were close to those of Dynabeads, which served as a positive control in the assay.

Molecule Release Profiles of PBMCs Activated with ccNPs-CD3/CD28. Cytokines play a critical role in shaping immune responses with distinct patterns of production being associated with specific T cell populations. We conducted a quantitative analysis of individual T-cell-related analytes by plotting the MFI measurements to a standard curve-plotting software to determine the concentration of each analyte.

The multianalyte flow assay performed allowed us to determine the following: (i) IFN-γ and TNF-α produced by T helper 1 (Th1) cells, IL-4 by Th2 cells, and IL-17 by Th17 cells; (ii) IL-10 secreted by regulatory T cells (Tregs), and (iii) perforin, granzymes A and B, and granulysin produced by cytotoxic T cells, which include CD8+ T cells and NK cells. Fas or CD95 is a membrane molecule expressed in most cells and can be produced as soluble Fas (sFas), by alternative splicing of the pre-mRNA; Fas L or CD178 is a proapoptotic molecule mainly expressed by T cells that can be processed at the transmembrane region (sFasL). Besides, monocytes also produce cytokines such as TNF-α and IL-10 or sFas molecules, whereas IFN-γ is also produced by CD8+ T cells and residual NK cells. This makes the analysis of molecule-released patterns a valuable tool for characterizing T cell activation.

We investigated the analyte production profiles in response to different stimuli in the supernatants of the PBMC proliferation assays ($n = 4$), collected after 5 days of stimulation (Figure 6). The inclusion of a standard solution of known concentration for each analyte enabled us to interpolate the MFI of the test samples based on those of the standard samples. Varied patterns of cytokine production were observed in response to the different stimuli used. ccNPs-CD3/CD28 induced maximal production of all three types of Th-related cytokines (IFN-γ, IL-4, and IL-17A) compared to the negative control ($p < 0.0001$), whereas ccNPs alone or decorated solely with the anti-CD3 antibody failed to elicit such a release (**$p < 0.01$, ***$p < 0.001$, and ****$p < 0.0001$) (Figure 6b). As expected, the concurrent presence of both TCR stimulatory and costimulatory signals was necessary for the full activation of this T cell subset. Concerning the cytotoxic-related analytes (Figure 6c), ccNPs-CD3/CD28 induced a considerable production, with levels comparable to those of the positive control. However, ccNPs and ccNPs-CD3 were, in general, unable to induce such a release. In summary, ccNPs-CD3/CD28 act as a polyclonal aAPCs, inducing the secretion of multiple signaling and effector molecules, with patterns and levels generally similar to those seen in the positive control.

High levels of IFN-γ and TNF-α can induce apoptosis in T cells by binding to the TNFR1 receptor instead of the TNFR2 receptor. Whereas TNF-α is increased in the presence of naive ccNPs relative to the negative control, the data revealed a very low production of IFN-γ. Despite, as described above, the levels of LPS in purified ccNPs being very low, we cannot completely discard a certain contribution to the TNF-α signal. However, we did not observe any bias in the results concerning T-cell activation that might point in this direction.

CONCLUSIONS

Herein, we employed biocompatible protein-only nanoparticles that can be easily and rapidly functionalized with an *a la carte* combination of antibodies in the desired ratio. This plug-and-play approach lays out on the use of ZapB-GFP-Z module, which is readily self-assembled intracellularly as a submicrometric α-helical-rich structure. After purification, the resulting nanostructured material offers multiple exposed Z-domain binding sites, enabling multivalent antibody display. Preassembled ccNPs can be easily produced and purified with high yields in a cost-effective manner. Overall, ccNPs exhibit advantages when compared with conventional polymeric and inorganic scaffolds, which require chemical conjugation, dispersion, or encapsulation to be functionalized with active protein moieties.

We demonstrate that ccNPs can be employed to create aAPCs by incorporating human anti-CD3 and anti-CD28 stimulatory cues into the particles by means of noncovalent and specific interactions with the Z-domain. ccNPs-CD3/CD28 induced in vitro polyclonal T cell proliferation and the expression of T cell activation markers. Furthermore, ccNPs-CD3/CD28 are capable of maintaining sustained cytokine production for a long period. The presence of multiple histidine tags in each ccNP might allow for its separation from the culture using Ni-NTA magnetic beads, if needed.

In conclusion, we describe the use of a biologically inspired protein-only nanostructure as an off-the-shelf product for in vitro T cell expansion and activation.

ASSOCIATED CONTENT

Supporting Information

The Supporting Information is available free of charge at https://pubs.acs.org/doi/10.1021/acsanm.4c00698.

Confocal microscopy images of ccNPs decorated with a combination of two fluorescently labeled antibodies, TEM imaging of ccNPs decorated with gold nanoparticle-conjugated antibodies, size distributions of naive ccNPs and ccNPs-CD3/CD28 measured by DLS over 5 days, zeta potential analysis of naive ccNPs and ccNPs-CD3/CD28, and results of the determination of the antibody loading capacity of ccNPs by fluorescence spectroscopy (PDF)

AUTHOR INFORMATION

Corresponding Authors

Javier Garcia-Pardo − *Institut de Biotecnologia i de Biomedicina (IBB), Universitat Autònoma de Barcelona, Bellaterra, Barcelona 08193, Spain; Departament de Bioquímica i Biologia Molecular, Universitat Autònoma de Barcelona, Bellaterra, Barcelona 08193, Spain*; Email: javiergarciapardo@msn.com

Mercè Martí − *Institut de Biotecnologia i de Biomedicina (IBB), Universitat Autònoma de Barcelona, Bellaterra, Barcelona 08193, Spain; Departament de Biologia Cel·lular, Fisiologia i Immunologia, Universitat Autònoma de Barcelona, Bellaterra, Barcelona 08193, Spain*; Email: Merce.Marti@uab.es

Salvador Ventura − *Institut de Biotecnologia i de Biomedicina (IBB), Universitat Autònoma de Barcelona, Bellaterra, Barcelona 08193, Spain; Departament de Bioquímica i Biologia Molecular, Universitat Autònoma de Barcelona,*

https://doi.org/10.1021/acsanm.4c00698
ACS Appl. Nano Mater. 2024, 7, 6669−6680

Bellaterra, Barcelona 08193, Spain; orcid.org/0000-0002-9652-6351; Email: Salvador.ventura@uab.cat

Authors

Marc Fornt-Suñé − *Institut de Biotecnologia i de Biomedicina (IBB), Universitat Autònoma de Barcelona, Bellaterra, Barcelona 08193, Spain; Departament de Bioquímica i Biologia Molecular, Universitat Autònoma de Barcelona, Bellaterra, Barcelona 08193, Spain*

Gonzalo Lázaro Bermejo − *Institut de Biotecnologia i de Biomedicina (IBB), Universitat Autònoma de Barcelona, Bellaterra, Barcelona 08193, Spain; Departament de Biologia Cel·lular, Fisiologia i Immunologia, Universitat Autònoma de Barcelona, Bellaterra, Barcelona 08193, Spain*

Marcos Gil-Garcia − *Institut de Biotecnologia i de Biomedicina (IBB), Universitat Autònoma de Barcelona, Bellaterra, Barcelona 08193, Spain; Departament de Bioquímica i Biologia Molecular, Universitat Autònoma de Barcelona, Bellaterra, Barcelona 08193, Spain*

Andrea Aran − *Institut de Biotecnologia i de Biomedicina (IBB), Universitat Autònoma de Barcelona, Bellaterra, Barcelona 08193, Spain; Departament de Biologia Cel·lular, Fisiologia i Immunologia, Universitat Autònoma de Barcelona, Bellaterra, Barcelona 08193, Spain*

Complete contact information is available at: https://pubs.acs.org/10.1021/acsanm.4c00698

Author Contributions

M.F.-S. and G.L.B. authors have contributed equally. S.V. designed the conceptual framework of the present work. M.F.-S., M.G.-G., J.G.-P., and S.V. designed the experiments related to the production, purification, characterization, and antibody-conjugation of the ccNPs. G.L.B., A.A., and M.M. designed the experiments related to the T cell proliferation assays, phenotypical characterization, and cytokine analysis. M.F.-S., G.L.B., M.G.-G., and A.A. performed the experiments. M.F.-S., G.L.B., J.G.-P., and M.M. analyzed the data and prepared the manuscript figures. M.F.-S., J.G.-P., and S.V. wrote the manuscript with contributions and valuable comments from all the authors.

Notes

The authors declare no competing financial interest.

■ ACKNOWLEDGMENTS

This work was funded by the Spanish Ministry of Science and Innovation (PID2019-105017RB-I00), by ICREA, ICREA-Academia 2020, to S.V., and by Fundación Contigo Contra el Cáncer de la Mujer (#BREASTILs. Functional Study of TILs from breast cancer patients: an approach to personalized medicine) to M.M. M.F.-S. was supported by the Spanish Ministry of Science and Innovation (FPU20/02897). G.L.B. was supported by the Universitat Autònoma de Barcelona (PIF 2021-22 B21P0025). M.G.-G. was supported by the Spanish Ministry of Science and Innovation (FPU16/02465). A.A. was supported by Fundación Contigo Contra el Cáncer de la Mujer. J.G-P. was supported by the Spanish Ministry of Science and Innovation with a Juan de la Cierva Incorporación IJC2019-041039-I. The authors thank the members of the Microscopy Service of the Universitat Autònoma de Barcelona for their technical support in electron microscopy and confocal imaging. We also thank the Cell Culture, Antibody Production and Cytometry Service and, specially, Manuela Costa for the technical support in Flow Cytometry analyses. We thank Andrea Livieri for her help in endotoxin measurements.

■ REFERENCES

(1) Waldman, A. D.; Fritz, J. M.; Lenardo, M. J. A Guide to Cancer Immunotherapy: From T Cell Basic Science to Clinical Practice. *Nat. Rev. Immunol.* **2020**, *20* (11), 651−668.

(2) Rosenberg, S. A.; Restifo, N. P. Adoptive Cell Transfer as Personalized Immunotherapy for Human Cancer. *Science* **2015**, *348* (6230), 62−68.

(3) Yee, C.; Lizee, G.; Schueneman, A. J. Endogenous T-Cell Therapy: Clinical Experience. *Cancer J.* **2015**, *21* (6), 492−500.

(4) Kuhns, M. S.; Badgandi, H. B. Piecing Together the Family Portrait of TCR-CD3 Complexes. *Immunol. Rev.* **2012**, *250* (1), 120−143.

(5) Huppa, J. B.; Davis, M. M. T-Cell-Antigen Recognition and the Immunological Synapse. *Nat. Rev. Immunol.* **2003**, *3* (12), 973−983.

(6) Esensten, J. H.; Helou, Y. A.; Chopra, G.; Weiss, A.; Bluestone, J. A. CD28 Costimulation: From Mechanism to Therapy. *Immunity* **2016**, *44* (5), 973−988.

(7) An, H.; Selvakumar, A.; O'Reilly, R. J. Artificial Antigen Presenting Cells: An Off the Shelf Approach for Generation of Desirable T-Cell Populations for Broad Application of Adoptive Immunotherapy. *Adv. Genet. Eng.* **2015**, *04* (03), 130.

(8) Kim, J. V.; Latouche, J.-B.; Rivière, I.; Sadelain, M. The ABCs of Artificial Antigen Presentation. *Nat. Biotechnol.* **2004**, *22* (4), 403−410.

(9) Gong, N.; Sheppard, N. C.; Billingsley, M. M.; June, C. H.; Mitchell, M. J. Nanomaterials for T-Cell Cancer Immunotherapy. *Nat. Nanotechnol.* **2021**, *16* (1), 25−36.

(10) Sunshine, J. C.; Green, J. J. Nanoengineering Approaches to the Design of Artificial Antigen-Presenting Cells. *Nanomedicine* **2013**, *8* (7), 1173−1189.

(11) Steenblock, E. R.; Wrzesinski, S. H.; Flavell, R. A.; Fahmy, T. M. Antigen Presentation on Artificial Acellular Substrates: Modular Systems for Flexible, Adaptable Immunotherapy. *Expert Opin. Biol. Ther.* **2009**, *9* (4), 451−464.

(12) Schluck, M.; Hammink, R.; Figdor, C. G.; Verdoes, M.; Weiden, J. Biomaterial-Based Activation and Expansion of Tumor-Specific T Cells. *Front. Immunol.* **2019**, *10*, 931.

(13) Hotaling, N. A.; Tang, L.; Irvine, D. J.; Babensee, J. E. Biomaterial Strategies for Immunomodulation. *Annu. Rev. Biomed. Eng.* **2015**, *17*, 317−349.

(14) Isser, A.; Livingston, N. K.; Schneck, J. P. Biomaterials to Enhance Antigen-Specific T Cell Expansion for Cancer Immunotherapy. *Biomaterials* **2021**, *268*, 120584.

(15) Eggermont, L. J.; Paulis, L. E.; Tel, J.; Figdor, C. G. Towards Efficient Cancer Immunotherapy: Advances in Developing Artificial Antigen-Presenting Cells. *Trends Biotechnol.* **2014**, *32* (9), 456−465.

(16) Perica, K.; Kosmides, A. K.; Schneck, J. P. Linking Form to Function: Biophysical Aspects of Artificial Antigen Presenting Cell Design. *Biochim. Biophys. Acta* **2015**, *1853* (4), 781−790.

(17) Rhodes, K. R.; Green, J. J. Nanoscale Artificial Antigen Presenting Cells for Cancer Immunotherapy. *Mol. Immunol.* **2018**, *98*, 13−18.

(18) Green, J. J.; Elisseeff, J. H. Mimicking Biological Functionality with Polymers for Biomedical Applications. *Nature* **2016**, *540* (7633), 386−394.

(19) Wauters, A. C.; Scheerstra, J. F.; Vermeijlen, I. G.; Hammink, R.; Schluck, M.; Woythe, L.; Wu, H.; Albertazzi, L.; Figdor, C. G.; Tel, J.; Abdelmohsen, L. K. E. A.; van Hest, J. C. M. Artificial Antigen-Presenting Cell Topology Dictates T Cell Activation. *ACS Nano* **2022**, *16* (9), 15072−15085.

(20) Cheung, A. S.; Zhang, D. K. Y.; Koshy, S. T.; Mooney, D. J. Scaffolds That Mimic Antigen-Presenting Cells Enable Ex Vivo Expansion of Primary T Cells. *Nat. Biotechnol.* **2018**, *36* (2), 160−169.

(21) Reisbeck, F.; Wedepohl, S.; Dimde, M.; Schmitt, A.-C.; Dernedde, J.; Álvaro-Benito, M.; Freund, C.; Haag, R. Synthesis and

Functionalization of Dendritic Polyglycerol-Based Nanogels: Application in T Cell Activation. *J. Mater. Chem. B* **2022**, *10* (1), 96−106.
(22) Lupas, A. N.; Bassler, J. Coiled Coils - A Model System for the 21st Century. *Trends Biochem. Sci.* **2017**, *42* (2), 130−140.
(23) Ebersbach, G.; Galli, E.; Møller-Jensen, J.; Löwe, J.; Gerdes, K. Novel Coiled-Coil Cell Division Factor ZapB Stimulates Z Ring Assembly and Cell Division. *Mol. Microbiol.* **2008**, *68* (3), 720−735.
(24) Tashiro, M.; Tejero, R.; Zimmerman, D. E.; Celda, B.; Nilsson, B.; Montelione, G. T. High-resolution solution NMR structure of the Z domain of staphylococcal protein A. *J. Mol. Biol.* **1997**, *272* (4), 573−590.
(25) Chen, C.; Huang, Q.-L.; Jiang, S.-H.; Pan, X.; Hua, Z.-C. Immobilized Protein ZZ, an Affinity Tool for Immunoglobulin Isolation and Immunological Experimentation. *Biotechnol. Appl. Biochem.* **2006**, *45* (2), 87−92.
(26) Gil-Garcia, M.; Ventura, S. Multifunctional Antibody-Conjugated Coiled-Coil Protein Nanoparticles for Selective Cell Targeting. *Acta Biomater.* **2021**, *131*, 472−482.
(27) Schneider, C. A.; Rasband, W. S.; Eliceiri, K. W. NIH Image to ImageJ: 25 Years of Image Analysis. *Nat. Methods* **2012**, *9* (7), 671−675.
(28) Carrió, M.; González-Montalbán, N.; Vera, A.; Villaverde, A.; Ventura, S. Amyloid-like Properties of Bacterial Inclusion Bodies. *J. Mol. Biol.* **2005**, *347* (5), 1025−1037.
(29) Gil-Garcia, M.; Ventura, S. Coiled-Coil Based Inclusion Bodies and Their Potential Applications. *Front. Bioeng. Biotechnol.* **2021**, *9*, 734068.
(30) de Groot, N. S.; Sabate, R.; Ventura, S. Amyloids in Bacterial Inclusion Bodies. *Trends Biochem. Sci.* **2009**, *34* (8), 408−416.
(31) Blundell, E. L. C. J.; Healey, M. J.; Holton, E.; Sivakumaran, M.; Manstana, S.; Platt, M. Characterisation of the Protein Corona Using Tunable Resistive Pulse Sensing: Determining the Change and Distribution of a Particle's Surface Charge. *Anal. Bioanal. Chem.* **2016**, *408* (21), 5757−5768.
(32) Chen, L.; Flies, D. B. Molecular Mechanisms of T Cell Co-Stimulation and Co-Inhibition. *Nat. Rev. Immunol.* **2013**, *13* (4), 227−242.
(33) Landmann, R.; Knopf, H. P.; Link, S.; Sansano, S.; Schumann, R.; Zimmerli, W. Human Monocyte CD14 Is Upregulated by Lipopolysaccharide. *Infect. Immun.* **1996**, *64* (5), 1762−1769.

https://doi.org/10.1021/acsanm.4c00698
ACS Appl. Nano Mater. 2024, 7, 6669−6680